Chapter 6

Modified SRF-PAC, Optimum Sizing of UPQC-DG and Hardware Validation

6.1 Preamble

Power angle control methods are effective in sharing VA burden between converters of UPQC-DG, but they tend to increase computational burden on the controller because estimation of power angle requires calculation of load active and reactive powers. In IRPT (p-q theory) based methods, load active and reactive powers are already known, so it is not additional burden [1–3]. In case of SRFT based methods proposed in previous chapters of this thesis have drawback of estimating load active and reactive powers additionally. A SRFT based PAC method (termed as 'SRF-PAC') for conventional UPQC proposed in [4], estimates load power using built-in SRF variables and avoids additional computation of load active and reactive powers, but it supports only small values of power angle because load power estimation is carried out in source voltage reference frame (which is true only for small value of power angle).

Proper design of UPQC-DG is a key factor for reduced cost, efficient operation and meeting stringent grid codes. Design of UPQC-DG includes sizing of series and shunt converters and series injection transformers. Since the shunt converter of UPQC-DG feeds power from DG, apart from supplying reactive power of load, its kVA rating becomes very high. So, Power Angle Control (PAC) method, aimed at sharing reactive power burden of shunt converter with series converter, has been devised [1–4].

Sizing of converters and transformer of UPQC with PAC is found to be optimal and less costly than conventional UPQC [5, 6]. In the case of UPQC-DG, various

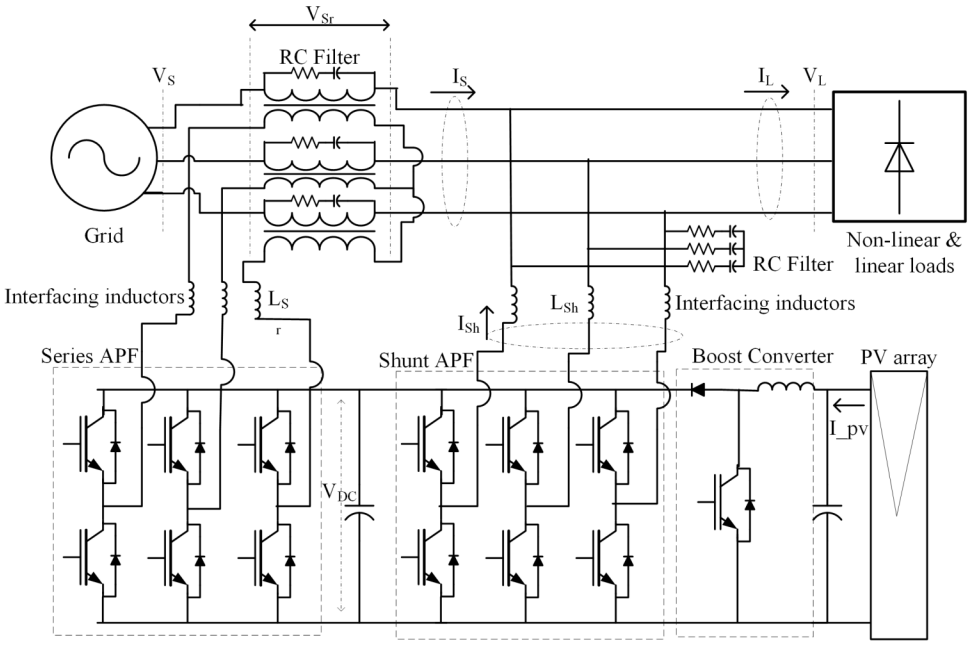

Figure 6.1: Configuration of three phase - three wire UPQC-DG without DC-DC converter

power angle control methods have been devised [1, 7, 8], but optimal sizing using PAC method has not been considered. Optimal sizing of UPQC-DG without PAC has been proposed but it leads to an increase in the size of shunt converter [9].

Once UPQC-DG converters have been optimally designed, the control strategy should ensure that converters operate within their designed ratings. PAC methods proposed so far, don't take into account the VA ratings of converters, though some methods do account for voltage rating of series APF [1, 10].

Therefore, in this chapter, a modified SRF-PAC method has been proposed to support larger values of power angle, which also avoids additional burden of computing load active and reactive powers. An optimal sizing method for UPQC-DG operating under PAC has been proposed. Lastly, an enhanced PAC method has been developed for ensuring VA loads of converter within the designed ratings for all operating conditions. Proposed design and control methods are presented with their application to a case study UPQC-DG system (with specific compensation requirements), but these are suitable for other types of UPQC-DG systems as well.

Section 6.2 presents case study system considered, section 6.3 explains optimal sizing of UPQC-DG using power angle control and section 6.4 deals with modified

SRF-PAC method proposed in this chapter. CHIL and hardware validation results of proposed methodology is presented in section 6.5 and section 6.6 respectively, and section 6.7 concludes the chapter.

6.2 Case Study System

In this work, a three-phase three wire UPQC-DG system has been considered. Grid and load parameters of case study system (PV based UPQC-DG) are shown in Table 6.1. A mix of reactive (R-L) and non-linear (rectifier) loads is taken to test performance of UPQC-DG in presence (or switching) of such loads.

As shown in Fig. 6.1, PV array is taken as DG, which can be directly connected to DC link without the use of DC-DC converter leading to the reduction in the number of power electronic interfaces, and thereby increasing system reliability. Such direct PV integration requires suitable design and control modifications in conventional UPQC-DG [11]. The output voltage of PV array at Maximum Power Point (MPP) is selected to match with DC link voltage of UPQC-DG. A diode is added to avoid reverse power flow into the PV array.

Table 6.1: Parameters of system

3-phase supply	415 V, 50 Hz, R_S = .08 Ω, L_S = 0.24 mH
Load-1	3-phase diode bridge rectifier (R_{DC} = 26 Ω)
Load-2	3-phase R-L load (20 kW, 0.707 p.f. lagging)
Load-3	3-phase R-L load (10 kW, 0.707 p.f. lagging)
PV array	P_{MPP} = 17.1 kW, V_{MPP} = 765 V

In conventional UPQC-DG (where PV is connected at DC link via DC-DC converter) systems DC link voltage is regulated at the constant reference value, but in case of UPQC-DG with direct PV integration, DC link voltage varies according to a variable reference value, which depends on MPP of PV array. PV array characteristics adopted in the present work are shown in Fig. 6.2. MPP of PV array at standard irradiation and temperature is 17.1 kW, and 765 V. Minimum DC link voltage should be larger than twice of the peak phase voltage, which is 678 V in the present system, and V_{MPP} of PV array is greater than 678 V for all practical irradiation values. Finally, the operating range of DC link voltage is taken as 700 to 740 V.

Primary compensation & PV integration requirements of UPQC-DG system are as follows:

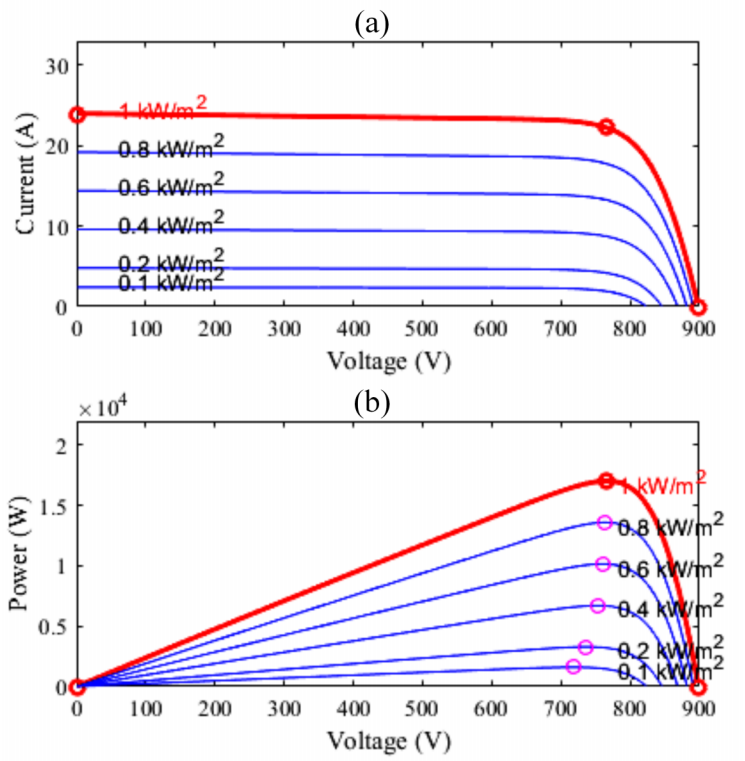

Figure 6.2: PV array (SunPower-SPR-305E-WHT-D, 4 parallel strings of 14 series modules) characteristics: (a) I-V curve, (b) P-V curve

1. Compensate for reactive load power and maintain unity power factor at the source.
2. Compensate for load current harmonics and maintain sinusoidal source current.
3. Compensate for source voltage sags and swells up to 40% of rated voltage.
4. Compensate for source voltage harmonics and maintain harmonic free load voltage.
5. Extract maximum power from PV and feed it to load.

6.3 Optimal Sizing of UPQC-DG

For optimizing the VA sizes of converters of UPQC-DG, its mathematical modeling is necessary, since it provides for formulation of optimization problem. Both, the mathematical modeling and optimization problems are discussed in following subsections.

6.3.1 Mathematical Modeling of UPQC-DG

This subsection establishes generic equations for VA load of series and shunt converters, and transformers of UPQC-DG, assuming that it is operating under PAC method. Phasor diagram of power angle controlled UPQC-DG under voltage sag is shown in Fig. 6.3. Though following equations have been derived for sag condition, these are equally applicable for swell or normal situations. Per phase VA load of series converter of UPQC-DG under voltage sag/swell is given by:

$$S_{Sr} = V_{Sr}.I_S' \tag{6.1}$$

V_{Sr} is per phase output voltage of series converter and I_S' is source current under sag/swell condition. Let source voltage changes by a factor k, which is less than unity for sag and greater than unity for swell. Using phasor diagram of UPQC-DG under PAC, series converter voltage can be expressed in terms of load voltage (V_L), power angle (δ), and change in source voltage (k):

$$V_{Sr} = V_L.\sqrt{1+k^2-2kcos\delta} \tag{6.2}$$

Ideally load power and power drawn from source remains constant under source voltage sag/swell, So source current changes in proportion to change in source voltage ($I_S' = I_S/k$). I_S is source current under steady state (no sag/swell). Using Eqs. 6.1 and 6.2, series converter VA load is given by:

$$S_{Sr} = V_L.\sqrt{1+k^2-2kcos\delta}.I_S/k \tag{6.3}$$

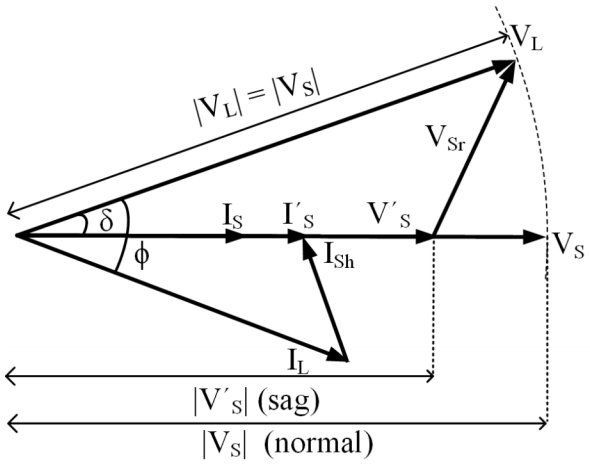

Figure 6.3: Phasor diagram under sag

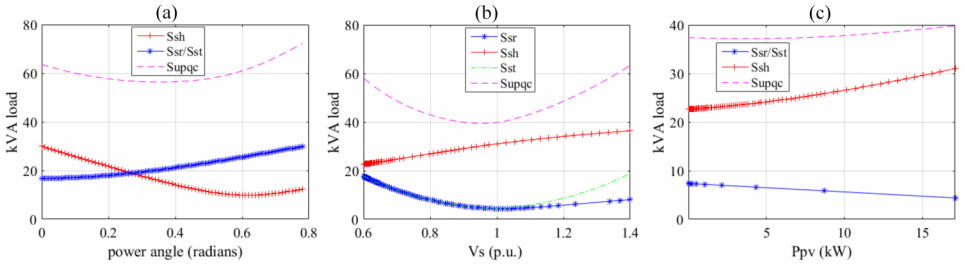

Figure 6.4: Typical kVA load curves of UPQC-DG (case-study system): (a) kVA loading for variation in power angle (δ) at 0.6 pu source voltage, full load and rated PV output, (b) kVA loading for variation in source voltage at $\delta = 10^{\circ}$, full load and rated PV output, (c) kVA loading for variation in solar PV output at $\delta = 10^{\circ}$, rated source voltage, full load.

Product $V_L.I_S = P_S$ represents active power drawn from source, which is equal to $P_L - P_{DG}$ ($P_{DG} = P_{PV}$, in the case under study). So, S_{Sr} is simplified:

$$S_{Sr} = \frac{(P_L - P_{DG}).\sqrt{1+k^2-2kcos\delta}}{k} \tag{6.4}$$

Since power loss of transformer is negligible, VA load of series injection transformer (S_T) will be equal to VA load on series converter (S_{Sr}). The rating of transformer will depend on maximum current and voltage:

$$S_T = \max(V_{Sr}).\max(I_S) \tag{6.5}$$

Per phase VA load of shunt converter under sag/swell is found as:

$$S_{Sh} = V_L.I_{Sh}{}' \tag{6.6}$$

Using phasor diagram, current supplied by shunt converter is expressed as:

$$I_{Sh}{}' = \sqrt{I_S{}'^2 + I_L{}^2 - 2.I_S{}'.I_L.cos(\phi - \delta)} \tag{6.7}$$

I_L is load current and ϕ is load power factor angle. Using Eq. 6.7, Eq. 6.6 is rearranged as $S_{Sh} =$

$$V_L.\sqrt{I_S'{}^2 + I_L{}^2 - 2I_S{}'I_L.(cos\phi.cos\delta + sin\phi.sin\delta)} \tag{6.8}$$

In terms of power quantities, VA load on shunt converter is simplified as

$$S_{Sh} = \sqrt{\left(\frac{P_S}{k}\right)^2 + S_L{}^2 - \frac{2.P_S.(P_L.cos\delta + Q_L.sin\delta)}{k}} \tag{6.9}$$

Typical kVA load curves of series & shunt converters, series transformer and their sum (the total kVA load of UPQC-DG) for variation of different design parameters of the case-study system have been drawn in Fig. 6.4. The curves in Fig. 6.4 are obtained using equations derived in present section. All the three parameters, namely power angle (δ), source voltage magnitude and PV power output effect the kVA load and need to be considered for sizing of UPQC-DG. Load has been taken as full load because the compensation requirements are maximum at full load. Nature of kVA load curves in Fig. 6.4 reveals that kVA loading of UPQC-DG is maximum at extreme points, which need specific attention while optimizing the size of UPQC-DG. So, constraints of optimization problem should be formulated accordingly.

6.3.2 Optimization Formulation

Main objective of sizing of any equipment is to reduce its cost, so components of UPQC-DG should be sized in such a way that overall cost is minimum. Let C_1 and C_2 be the costs/VA of converter and transformer respectively. Then overall cost of UPQC-DG for minimization problem is given by Eq. 6.10. Since VA load of converters and transformer is maximum during sag/swell conditions, it should be ensured that VA load during these don't exceed beyond their ratings. In case of

Table 6.2: Comparison of VA ratings obtained using existing and proposed methods

Method	S_{Sr} (kVA)	S_{Sh} (kVA)	S_T (kVA)	$V_{Sr,rated}$ (V)	Total cost (USD)
1. Conventional [12]	28.20	41.17	28.20	95.84	118166
2. Existing PAC [1]	28.40	39.80	28.40	119.7	116512
3. Proposed Method	29.22	34.09	29.22	166.67	109586

UPQC-DG a special care needs to be taken because change in DG power result in still higher VA load of the components of UPQC-DG. Considering these worst case scenarios, the constraints on optimization are defined in Eqs. 6.11-6.22. Current $I_S{}^*$ in Eqs. 6.19 and 6.22 refers to source current during steady state with minimum power injection from DG.

$$\text{min. } F_1 = C_1.(S_{Sr,Rated} + S_{Sh,Rated}) + C_2.S_{T,Rated} \tag{6.10}$$

$$\text{Subject to } S_{Sr,Rated} \geq S_{Sr}(k_{min}, \delta_1, P_{DG,max}) \tag{6.11}$$
$$S_{Sh,Rated} \geq S_{Sh}(k_{min}, \delta_1, P_{DG,max}) \tag{6.12}$$
$$S_{T,Rated} \geq V_{Sr}(k_{min}, \delta_1).I_S/k_{min} \tag{6.13}$$
$$S_{Sr,Rated} \geq S_{Sr}(k_{max}, \delta_2, P_{DG,max}) \tag{6.14}$$
$$S_{Sh,Rated} \geq S_{Sh}(k_{max}, \delta_2, P_{DG,max}) \tag{6.15}$$
$$S_{T,Rated} \geq V_{Sr}(k_{max}, \delta_2).I_S/k_{min} \tag{6.16}$$
$$S_{Sr,Rated} \geq S_{Sr}(k_{min}, \delta_3, P_{DG,min}) \tag{6.17}$$
$$S_{Sh,Rated} \geq S_{Sh}(k_{min}, \delta_3, P_{DG,min}) \tag{6.18}$$
$$S_{T,Rated} \geq V_{Sr}(k_{min}, \delta_3).I_S{}^*/k_{min} \tag{6.19}$$
$$S_{Sr,Rated} \geq S_{Sr}(k_{max}, \delta_4, P_{DG,min}) \tag{6.20}$$
$$S_{Sh,Rated} \geq S_{Sh}(k_{max}, \delta_4, P_{DG,min}) \tag{6.21}$$
$$S_{T,Rated} \geq V_{Sr}(k_{max}, \delta_4).I_S{}^*/k_{min} \tag{6.22}$$

The optimization problem mentioned above is a smooth non-linear optimization

and can be solved using Non-Linear Programming (NLP) methods. Controlled variables in NLP are $S_{Sr,Rated}$, $S_{Sh,Rated}$, $S_{T,Rated}$, δ_1, δ_2, δ_3, δ_4. Upper limits on these controlled variables are chosen based on system requirements. Since sizing of UPQC-DG is an off-line procedure, any of the off-line optimization tools can be employed for solving the above optimization problem. In this work interior-point method [13] using MATLAB has been adopted. The values of C_1 and C_2 are taken as \$1.501/VA and \$0.498/VA [5].

For case study system, VA ratings for series and shunt converters as wells transformer have been obtained using proposed design method, and the results are compared with those obtained using existing PAC method of UPQC-DG [1], and conventional (without PAC) approach [12], and results are shown in Table 6.2. Total kVA ratings for all three phases of corresponding converters are presented instead of kVA ratings per phase. The proposed sizing method outperforms both methods and gives 7.26%, & 5.94% reduction in total cost compared to sizing with the conventional (without PAC) approach, and existing PAC method respectively. Existing PAC method of UPQC-DG doesn't provide a significant improvement in cost because the reduction in shunt converter rating is not enough to compensate for increase of series converter rating.

6.4 UPQC-DG Controller

Since ratings of UPQC-DG have been optimally designed, power angle control needs to be accordingly developed so that none of the converters and transformer exceed their ratings for any of the operating conditions of UPQC-DG. Conventional power angle control methods don't account for VA limitations, so in this work a modified power angle control has been devised which incorporates VA limitations. Control of each of the converters is described in detail as follows:

6.4.1 Shunt Converter Control

In the present work, Synchronous Reference Frame (SRF) theory based extraction has been employed to generate reference compensating currents for shunt converter (Fig. 6.5). In this method, Park's transform (Eq. 6.23) converts three phase load currents from abc frame to dq0 frame. This transforms fundamental components of three phase load currents into DC counterparts. These DC quantities can be easily

extracted using mean (moving average) blocks. Mean d-axis load current ($\bar{I}_{Ld}$) represents fundamental component of load current, which is in-phase with load voltage. Mean q-axis load current ($\bar{I}_{Lq}$) represents fundamental component of load current, which is out of phase with load voltage. Alternatively, $\bar{I}_{Ld}$ represents load active power, and $\bar{I}_{Lq}$ represents load reactive power.

$$\begin{bmatrix} I_{Ld} \\ I_{Lq} \\ I_{L0} \end{bmatrix} = \frac{2}{3} \begin{bmatrix} sin\alpha t & sin(\alpha t - \frac{2\pi}{3}) & sin(\alpha t + \frac{2\pi}{3}) \\ cos\alpha t & cos(\alpha t - \frac{2\pi}{3}) & cos(\alpha t + \frac{2\pi}{3}) \\ 1/2 & 1/2 & 1/2 \end{bmatrix} \begin{bmatrix} I_{La} \\ I_{Lb} \\ I_{Lc} \end{bmatrix} \tag{6.23}$$

DC link voltage regulation requires a suitable DC current (I_{DC}) to be supplied to DC capacitor. I_{DC} represents power losses in UPQC and is estimated using a PI controller. Perturb and Observe (P&O) technique based Maximum Power Point Tracking (MPPT) method computes the reference value of the DC link voltage.

PV output current (I_{PV}) is subtracted from sum of $\bar{I}_{Ld}$ and I_{DC} to form reference d-axis supply current(I_d^*). Inverse Park's transform (Eq. 6.23) is used to get balanced, sinusoidal reference source currents, which are compared with respective measured source currents in hysteresis controller to generate switching pulses.

Park and inverse-Park transforms require a ramp signal synchronized with reference AC sinusoidal signal. For inverse-Park, the source voltage is used as the reference signal because the source current is required to be in phase with the source voltage. In Eq. 6.23, ideally, load voltage should be used as the reference signal because load active and reactive powers are defined in the load voltage reference frame. In conventional UPQC control (without PAC), taking supply voltage as reference signal in Eq. 6.23 works well because load voltage is in phase with supply voltage.

However, in PAC method, load voltage leads supply voltage by power angle (Fig. 6.3). SRF-PAC method proposed in [4], uses supply voltage as the reference voltage in Eq. 6.23, which is acceptable only for small values of power angle. The present work proposes to use load voltage as the reference signal in Park's transform for larger power angles. To avoid using extra Phase Locked Loop (PLL) on load voltage, the present work proposes to add power angle to *wt* available from PLL applied on supply voltages, which gives ramp signal (αt) in synchronism with load voltage (Fig. 6.5).

Above mentioned drawback of existing SRF-PAC ([4]) and the improvement provided by proposed modified SRF-PAC are also proven mathematically as follows.

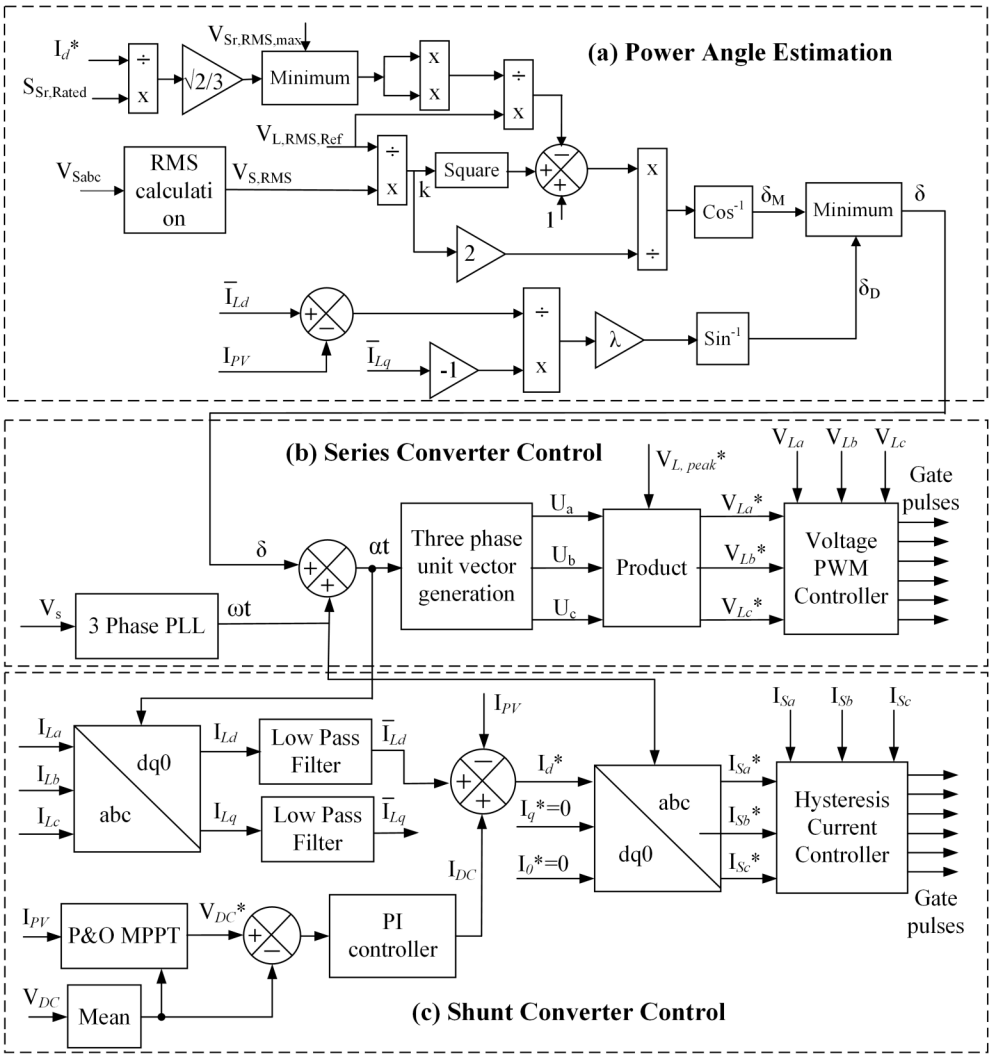

Figure 6.5: Modified Power Angle Control of UPQC-DG

In UPQC under PAC approach, the three phase load currents for a balanced inductive load, lag behind the load voltages (which lead source voltages by power angle):

$$\begin{bmatrix} I_{La} \\ I_{Lb} \\ I_{Lc} \end{bmatrix} = \begin{bmatrix} I_m sin(\omega t + \delta - \phi) \\ I_m sin(\omega t + \delta - 2\pi/3 - \phi) \\ I_m sin(\omega t + \delta + 2\pi/3 - \phi) \end{bmatrix} \tag{6.24}$$

In Eq. 6.24, I_m is amplitude of load current and ϕ is power factor angle. In existing SRF-PAC, I_{Ld} is calculated using Eq. 6.23 (with $\alpha t = \omega t$) &6.24:

$$\begin{aligned} I_{Ld} = \frac{2}{3}[&I_m sin(\omega t + \delta - \phi) sin(\omega t) + \\ &I_m sin(\omega t - \frac{2\pi}{3} + \delta - \phi) sin(\omega t - \frac{2\pi}{3}) + \\ &I_m sin(\omega t + \frac{2\pi}{3} + \delta - \phi) sin(\omega t + \frac{2\pi}{3})] \end{aligned} \tag{6.25}$$

Eq. 6.25 is simplified using product to sum trigonometric formula:

$$\begin{aligned} I_{Ld} = \frac{I_m}{3}[&cos(\delta - \phi) - cos(2\omega t + \delta - \phi) + \\ &cos(\delta - \phi) - cos(2\omega t + \delta - \phi - \frac{4\pi}{3}) + \\ &cos(\delta - \phi) - cos(2\omega t + \delta - \phi + \frac{4\pi}{3})] \end{aligned} \tag{6.26}$$

After simplification, Eq. 6.26 results in:

$$I_{Ld} = I_m cos(\phi - \delta) \tag{6.27}$$

Active power of load is $(3/2)V_m I_m cos\phi$ (V_m is amplitude of load voltage), and corresponding in phase component of current is $I_m cos\phi$. So, I_{Ld} found using existing SRF-PAC doesn't give correct estimation of in-phase component of load current.

Similarly, I_{Lq} is found in existing SRF-PAC based on Eq. 6.23 and 6.24:

$$\begin{aligned} I_{Lq} = \frac{2}{3}[&I_m sin(\omega t + \delta - \phi) cos(\omega t) + \\ &I_m sin(\omega t - \frac{2\pi}{3} + \delta - \phi) cos(\omega t - \frac{2\pi}{3}) + \\ &I_m sin(\omega t + \frac{2\pi}{3} + \delta - \phi) cos(\omega t + \frac{2\pi}{3})] \end{aligned} \tag{6.28}$$

$$\begin{aligned} I_{Lq} = \frac{I_m}{3}[&sin(2\omega t + \delta - \phi) + sin(\delta - \phi) + \\ &sin(2\omega t + \delta - \phi - \frac{4\pi}{3}) + sin(\delta - \phi) + \\ &sin(2\omega t + \delta - \phi + \frac{4\pi}{3}) + sin(\delta - \phi)] \end{aligned} \tag{6.29}$$

$$I_{Lq} = I_m sin(\delta - \phi) \tag{6.30}$$

Reactive power of three phase load is $(3/2)V_m I_m sin\phi$ and corresponding out of phase component is $I_m sin\phi$, which is not represented by I_{Lq} in existing approach.

In proposed modified SRF-PAC, αt is taken as $\omega t + \delta$, which is actual phasor position of load voltage with respect to source voltage (the reference phasor in both approaches). With this modification, I_{Ld} is found using Eq. 6.23 and 6.24:

$$\begin{aligned} I_{Ld} = \frac{2}{3}[&I_m sin(\omega t + \delta - \phi) sin(\omega t + \delta) + \\ &I_m sin(\omega t - \frac{2\pi}{3} + \delta - \phi) sin(\omega t + \delta - \frac{2\pi}{3}) + \\ &I_m sin(\omega t + \frac{2\pi}{3} + \delta - \phi) sin(\omega t + \delta + \frac{2\pi}{3})] \end{aligned} \tag{6.31}$$

Simplification of Eq. 6.31 results in:

$$\begin{aligned} I_{Ld} = \frac{I_m}{3}[&cos(\phi) - cos(2\omega t + 2\delta - \phi) + \\ &cos(\phi) - cos(2\omega t + 2\delta - \phi - \frac{4\pi}{3}) + \\ &cos(\phi) - cos(2\omega t + 2\delta - \phi + \frac{4\pi}{3})] \end{aligned} \tag{6.32}$$

$$I_{Ld} = I_m cos\phi \tag{6.33}$$

So, I_{Ld} found in proposed method corresponds to in-phase component of load current, or the active power of load.

Similarly I_{Lq} is also calculated using Eq. 6.23 and 6.24 based on proposed approach:

$$\begin{aligned} I_{Lq} = \frac{2}{3}[&I_m sin(\omega t + \delta - \phi) cos(\omega t + \delta) + \\ &I_m sin(\omega t - \frac{2\pi}{3} + \delta - \phi) cos(\omega t + \delta - \frac{2\pi}{3}) + \\ &I_m sin(\omega t + \frac{2\pi}{3} + \delta - \phi) cos(\omega t + \delta + \frac{2\pi}{3})] \end{aligned} \tag{6.34}$$

$$\begin{aligned} I_{Lq} = \frac{I_m}{3}[&sin(2\omega t + 2\delta - \phi) - sin(\phi) + \\ &sin(2\omega t + 2\delta - \phi - \frac{4\pi}{3}) - sin(\phi) + \\ &sin(2\omega t + 2\delta - \phi + \frac{4\pi}{3}) - sin(\phi)] \end{aligned} \tag{6.35}$$

$$I_{Lq} = -I_m sin\phi \tag{6.36}$$

So, I_{Lq} in proposed approach corresponds of magnitude of out of phase component of load current or load reactive power.

6.4.2 Series Converter control

In PAC method, series converter supplies a part of reactive power demand of load, for which, series voltage needs to be injected in quadrature with source current, resulting in phase difference (power angle) between supply and load voltage. Magnitude of series voltage (and reactive power supplied by series converter) depends on power angle, which is calculated using Eq. 6.37 [1]:

$$\delta_D = \sin^{-1}\left(\frac{Q_{Sr}}{P_L - P_{DG}}\right) = \sin^{-1}\left(\frac{Q_{Sr}}{P_L - P_{PV}}\right) \tag{6.37}$$

If reactive power is shared in proportion to VA ratings of converters then, reactive power delivered by series converter is estimated using Eq. 6.38, where Q_L is load reactive power and λ is ratio of VA rating of series converter to sum of VA ratings of two converters. Finally, desired power angle is found using Eq. 6.39.

$$Q_{Sr} = \frac{Q_L S_{Sr,rated}}{S_{Sr,rated} + S_{Sh,rated}} = \lambda Q_L \tag{6.38}$$

$$\delta_D = \sin^{-1}\left(\frac{\lambda Q_L}{P_L - P_{PV}}\right) \tag{6.39}$$

Upper limit on power angle is decided by voltage and kVA ratings of series converter. From phasor diagram maximum allowable power angle is found in Eq. 6.40, where k'_{max} is the ratio of maximum series converter voltage to reference load voltage.

$$\delta_M = \cos^{-1}\left[\frac{1 + k^2 - {k'_{max}}^2}{2k}\right] \tag{6.40}$$

Eq. 6.40 takes care of only voltage limit of series converter, and not its VA limit. To incorporate VA limit of series converter, present work proposes a modified estimation of voltage limit of series converter from series converter current (which is equal to source current for unity turns ratio of series injection transformer):

$$k''_{max} = \frac{S_{Sr,rated}}{3 I_S V_L} \tag{6.41}$$

Since at small source currents, k''_{max} can exceed rated voltage ratio, better approach is to estimate it using Eq. 6.42, which takes care of both voltage and VA limits:

$$k'_{max} = min. \left(\frac{S_{Sr,rated}}{3I_S V_L}, \frac{V_{Sr,rated}}{V_L} \right) \tag{6.42}$$

So, maximum value of power angle meeting both the voltage and VA limits of series converter is given by Eq. 6.40:

$$\delta_M = \cos^{-1} \left[\frac{1 + k^2 - \left[min. \left(\frac{S_{Sr,rated}}{3I_S V_L}, \frac{V_{Sr,rated}}{V_L} \right) \right]^2}{2k} \right] \tag{6.43}$$

Block diagram of SRF based power angle estimation is shown in Fig. 6.5(a). At each instant, power angle is calculated using Eq. 6.39, which demands estimation of real and reactive powers consumed by load. For a balanced three phase load, real power is computed from d-q frame quantities using Eq. 6.44:

$$P_L = \frac{3}{2} \overline{V}_{Ld} \bar{I}_{Ld} \tag{6.44}$$

Similarly load reactive power is estimated using Eq. 6.45:

$$Q_L = -\frac{3}{2} \overline{V}_{Ld} \bar{I}_{Lq} \tag{6.45}$$

Thus, a simple relationship for computing power angle is obtained from Eq. 6.39, in which $\bar{I}_{Ld}$ and $\bar{I}_{Lq}$ are obtained from shunt converter control loop:

$$\delta_D = \sin^{-1} \left(\frac{-\lambda \bar{I}_{Lq}}{\bar{I}_{Ld} - I_{PV}} \right) \tag{6.46}$$

Also, maximum limit on power angle computation is simplified in SRF based method. RMS calculation for source current is avoided by making use of ($I_d{}^*$) from shunt converter control, since for harmonic free three-phase signal, peak value equals its d-component in d-q frame. So, RMS source current is found using Eq. 6.47.

$$I_S = \frac{I_d{}^*}{\sqrt{2}} \tag{6.47}$$

So, in SRF based control maximum power angle computation is performed using Eq. 6.48

$$\delta_M = \cos^{-1}\left[\frac{1+k^2-\left[min.\left(\frac{\sqrt{2}S_{Sr,rated}}{3I_d{}^*V_L},\frac{V_{Sr,rated}}{V_L}\right)\right]^2}{2k}\right] \tag{6.48}$$

The final power angle (δ) is minimum of desired power angle (δ_D) and maximum power angle (δ_M).

In this chapter, the Unit Vector Template Generation (UVTG) technique [14] has been used for producing reference signals of the series converter (Fig. 6.5). Generated three phase unit vectors are amplified by taking their product with the desired amplitude of load voltage. The resultant three phase time-varying quantities serve as reference load voltage signals, which are compared with their respective measured counterparts in a PWM controller, which produces switching pulses.

6.5 Controller Hardware in Loop Validation

Validation of the proposed design and control method has been performed using Controller Hardware in Loop approach (CHIL) (Fig. 6.6). Proposed control algorithm has been implemented in Dspace/micro-labbox, and plant of case study system has been implemented on real-time simulator Opal-RT OP-4510. Sample time used for the controller is 25 μs and plant runs on fast FPGA based computational engine of Opal-RT with 0.5 μs time step. Measurements from the plant are taken from analog outputs of Opal-RT and passed to analog inputs of the controller. The controller provides PWM pulses at its digital output port which connects to the digital input port of Opal-RT. The values of interfacing inductors and RC filters, used at output of converters, have been selected using method given in [12].

In steady state, all three loads are ON, and the resultant load current is non-linear and reactive (Fig. 6.7(a-c)). Shunt converter compensates for non-linear components of load current. Shunt and series converters share reactive power burden in proportion to their VA ratings. Eventually source current is found to be sinusoidal and in phase with the source voltage. Load current THD in steady state is 7.51% and after compensation by shunt converter, the source current THD is 2.51% (which is below 5% limit as per IEEE-519 standard). Shunt converter also supplies active power injected by PV, which operates at its rated value (at $1000W/m^2$, $25°C$).

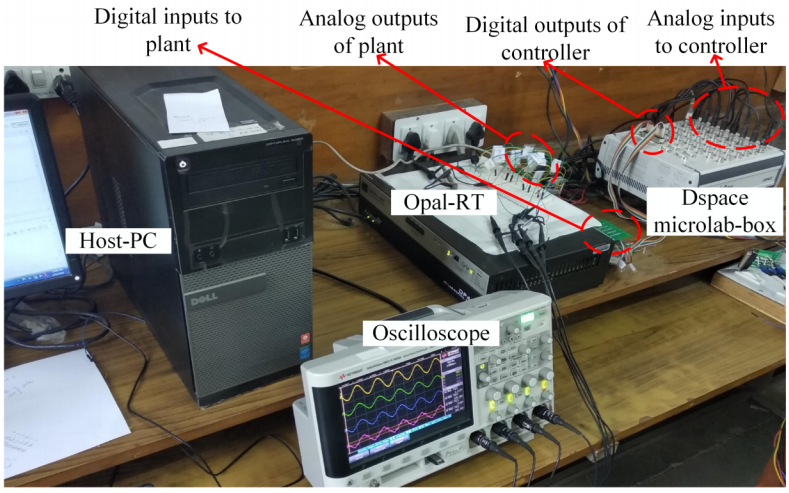

Figure 6.6: CHIL setup for validation of proposed control

Table 6.3: Variation in power angle & loading of components of UPQC-DG under different operating conditions for proposed PAC method

Operating condition	δ (°)	S_{Sr} (kVA)	S_{Sh} (kVA)	V_{Sr} (V)
1. Steady state with full load & full PV	25.0	12.2	27.6	106
2. Steady state with full load & nil PV	18.1	13.8	16.3	77
3. Steady state with load-3 off & full PV	23.8	7.2	22.7	103
4. Steady state with full load & 60% PV	21.7	12.7	21.5	92
5. 40% Voltage sag with full load & full PV	25.9	21.5	12.8	121
6. 40% Voltage swell with full load & full PV	26.5	12.7	34.0	161
7. 40% Voltage sag with full load & nil PV	8.1	28.7	33.8	96
8. 40% Voltage swell with full load & nil PV	18.4	17.4	25.2	130

Table 6.4: Variation in power angle & loading of components of UPQC-DG under different operating conditions for existing PAC [1]

Operating condition	δ (°)	S_{Sr} (kVA)	S_{Sh} (kVA)	V_{Sr} (V)
1. Steady state with full load & full PV	12.0	5.4	30.3	52.1
2. Steady state with full load & nil PV	12.1	8.6	21.7	77
3. Steady state with load-3 off & full PV	0.0	0.3	26.3	4.7
4. Steady state with full load & 60% PV	12.2	6.8	25.8	50.4
5. 40% Voltage sag with full load & full PV	6.7	16.2	24.2	96.2
6. 40% Voltage swell with full load & full PV	0.0	7.3	39.8	91.2
7. 40% Voltage sag with full load & nil PV	6.3	28.4	36.2	96.0
8. 40% Voltage swell with full load & nil PV	0.0	11.8	33.4	90.5

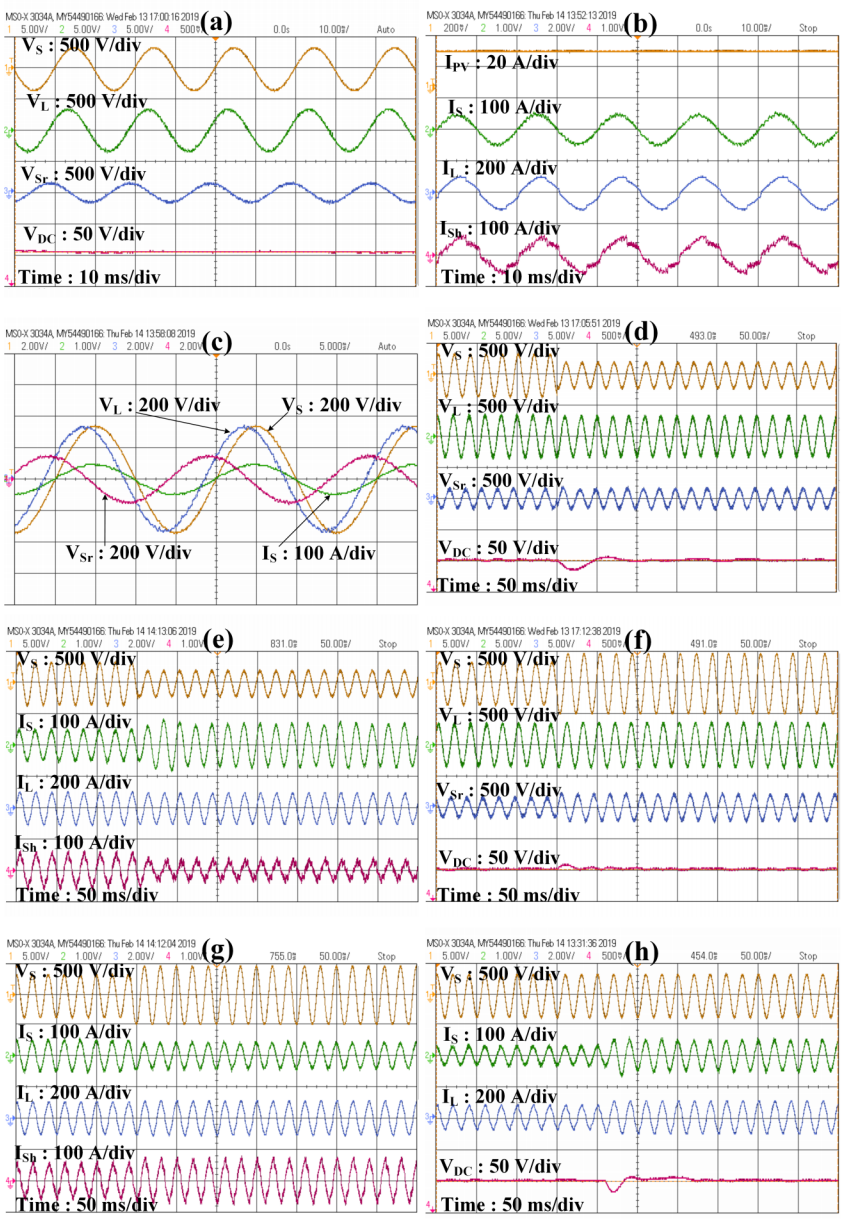

Figure 6.7: CHIL results of proposed UPQC-DG: (a) steady-state voltages, (b) steady-state currents, (c) phasor relationshp between key quantities, (d) voltages during sag, (e) currents during sag, (f) voltages during swell, (g) currents during swell, (h) performance during load-change

Occurrence of voltage sag and swell is simulated at full load and full PV output. During sag and swell (both of which are 40% of source voltage), load voltage is

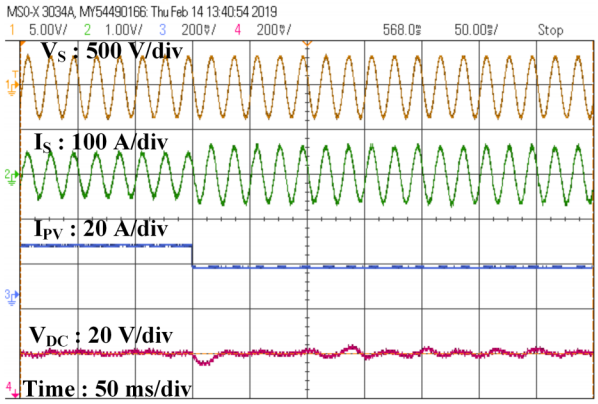

Figure 6.8: Performance during change in solar irradiation

maintained at its reference value by suitable modification of phase and magnitude of series converter voltage (Fig. 6.7(d-g)). On the occurrence of sag, DC link voltage experiences an undershoot of 17 V (2.3%), and at the instant of swell, it undergoes overshoot of 11 V (1.5%). Source current changes according to change in source voltage to supply the required amount of power to load.

Change of load is simulated as the transition from partially loaded condition (load 1 and 2 connected) to fully loaded condition (all loads are connected) and PV operating at its rating. During the rise in load, source current is increased to cater to greater active power demand (Fig. 6.7(h)). DC link voltage experiences an undershoot of 18 V (2.5%) and settles within 1% of the steady state in 81 ms. After the reduction in linear load, THD of the load current is found to be 10.15% and source current THD is 3.66% (remains under 5%).

To observe the effect of variation in solar irradiation, the irradiation is reduced by 40% in step fashion (worst case) while the system was in the steady state (Fig. 6.8). As a result, active power injected by PV array reduces and source current increases to compensate for this decrease. DC link voltage experiences an undershoot and oscillations of small magnitudes (both less than 1% of the steady state).

The variations in power angle, VA loading of series and shunt converters, and series converter output voltage under different operating conditions of UPQC-DG for proposed method are shown in Table 6.3 (VA loads shown are considering all three phases). Under all operating conditions, these values are kept within their designed ratings using the proposed control method. Shunt converter is fully loaded during

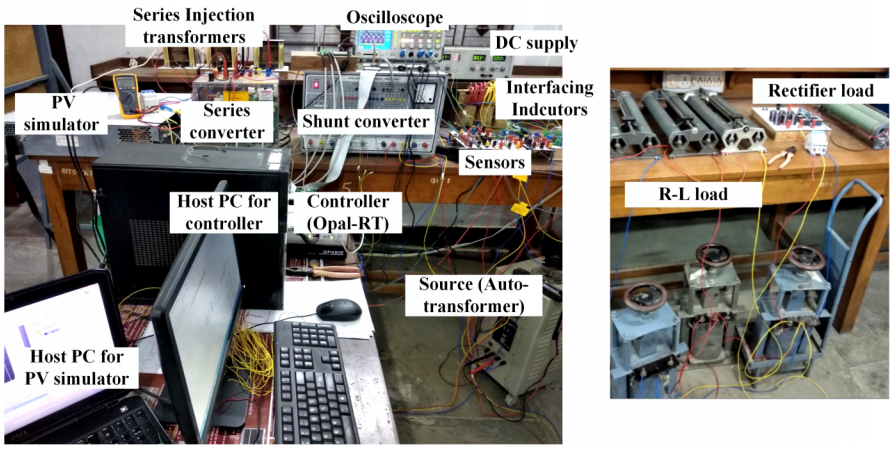

Figure 6.9: Hardware setup for experimental validation of proposed control

40% swell in source voltage when PV power output is also at peak. The series converter has maximum VA loading during 40% sag in source voltage when PV power output is nil. In case of reference PAC method (Table 6.4), the VA load on shunt converter violates its rating for voltage swell with full PV output (case-6) and voltage sag with nil PV generation (case-7), because VA limitations are not taken care in control loop of reference method. Also, in reference PAC method, the series converter utilization in the steady-state and most of transient states is less compared to shunt converter leading to uneven distribution of VA burden.

6.6 Hardware Validation

Experimental validation of developed modified SRF-PAC method has been carried using laboratory based power hardware setup (Fig. 6.9). Ratings of hardware setup,

Table 6.5: Specifications of UPQC-DG prototype

Supply	80 V, 3-phase, 50 Hz
Load-1	3-phase uncontrolled rectifier (R_{DC} = 90.0 Ω)
Load-2	R_Y = 16.8 Ω/phase, L_Y = 62.4 mH/phase
PV array	P_{MPP} = 102 W, V_{MPP} = 150 V, V_{OC} = 175 V, I_{SC} = 0.72 A
DC link	V_{DC} = 150 V, C_{DC} = 1150 μF
Shunt APF	$S_{Sh,rated}$ = 212.0 VA, L_{Sh} = 5.5 mH
Series APF	$S_{Sr,rated}$ = 204.0 VA, L_{Sr} = 7.0 mH
Series Transformer	n_T = 2 (100/50 V), $S_{T,rated}$ = 204.0 VA

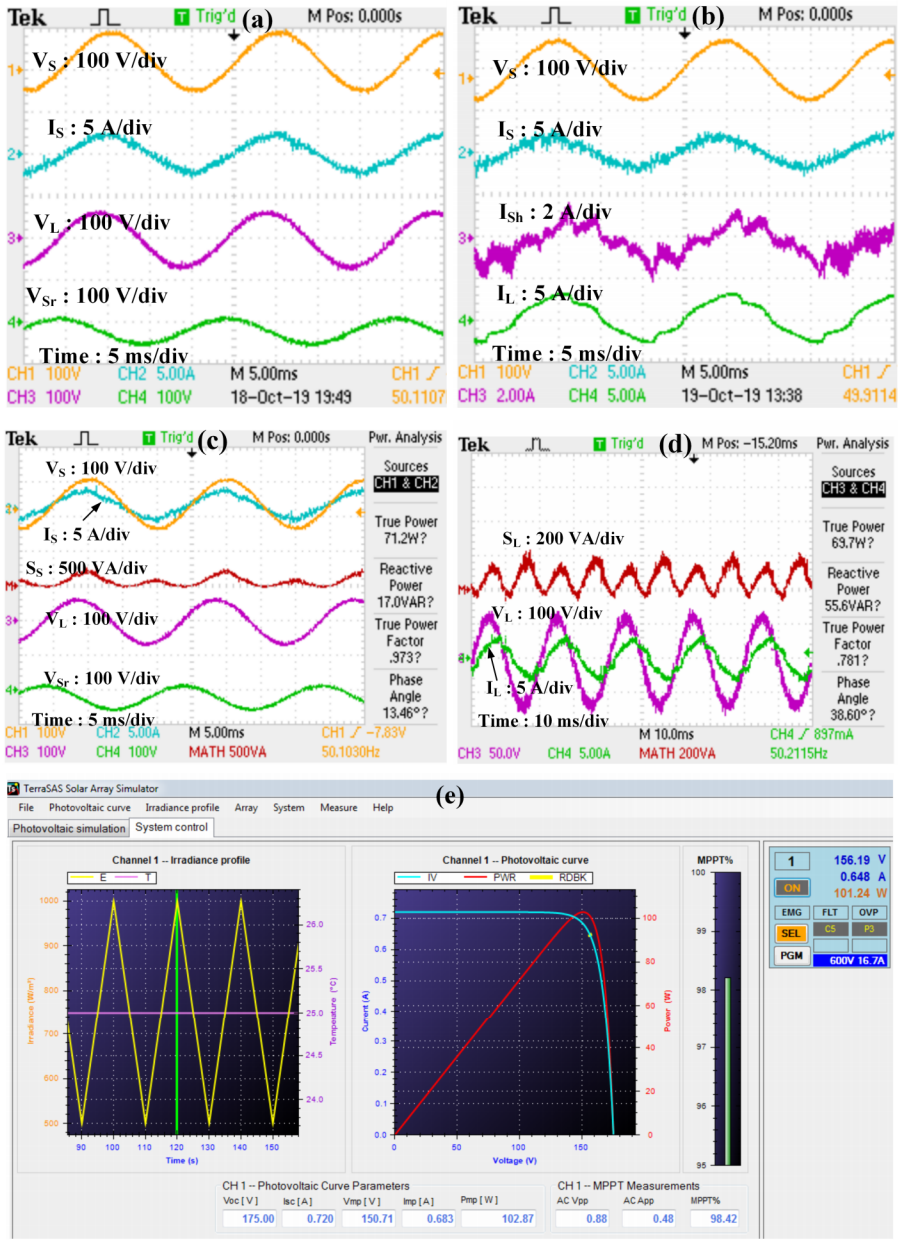

Figure 6.10: Experimental results of proposed UPQC-DG control: (a) key waveforms obtained in proposed modified SRF-PAC, (b) shunt compensation waveforms, (c) source power factor (d) load power factor (e) PV array simulator control panel

given in Table. 6.5, are chosen smaller than those of CHIL because of limitations of lab equipment. Design of converters of UPQC-DG has been carried out using the optimum sizing approach proposed in this chapter. PV array with ratings suitable to

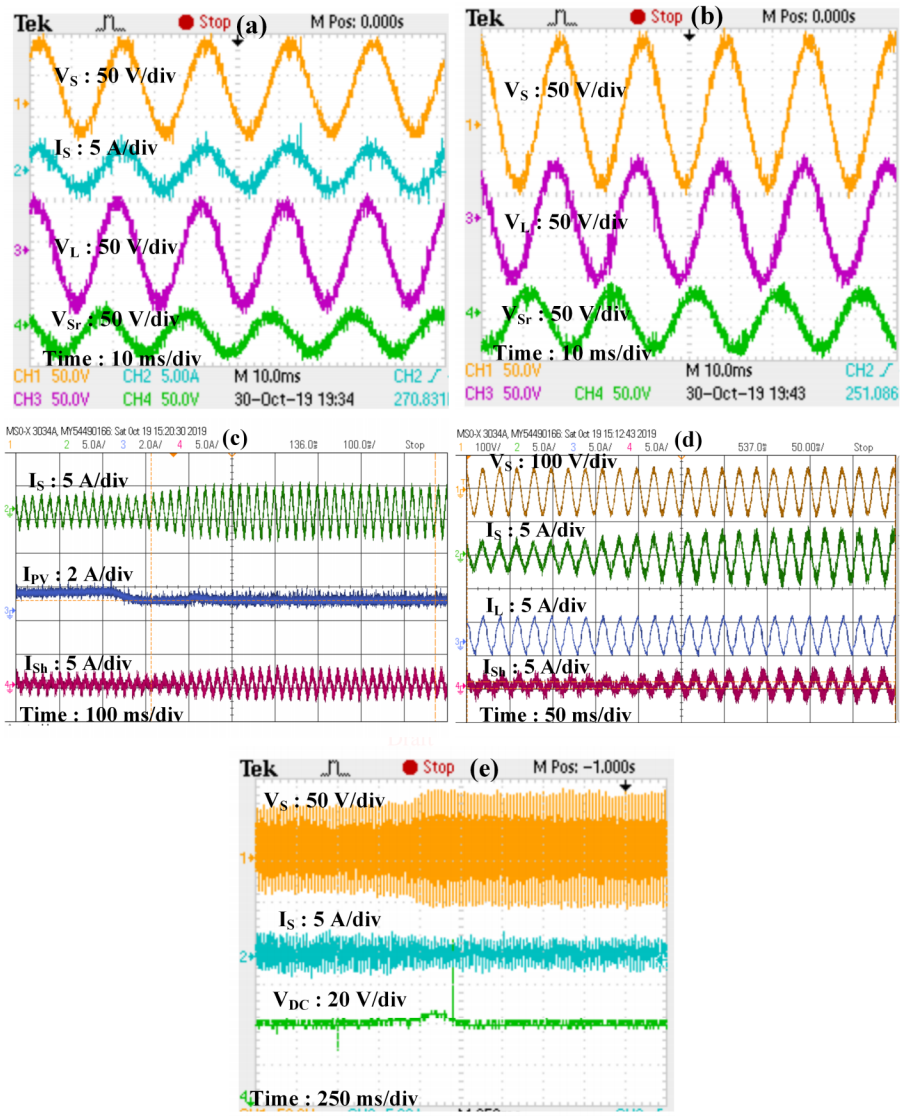

Figure 6.11: Experimental results of proposed UPQC-DG control: (a) performance during swell, (b) performance during swell, (c) reduction in solar irradiation (d) other waveforms during reduction in irradiation (e) DC link dynamics

direct interfacing on DC link has been simulated using TerrSAS PV array simulator. Opal-RT OP4510 has been used as real time controller for implementing proposed control along with PWM generation and measurement processing. Sampling time of controller is kept as 15 μs.

6.6.1 Steady State Results

Results of experimental validation are given in Fig. 6.10. In steady state, series APF of UPQC participates in reactive power compensation, so, series APF voltage is in quadrature with source current and load voltage leads source voltage. Steady state shunt compensation in proposed control is shown in Fig. 6.10(b), where shunt APF compensates for reactive (partly) and harmonic components of load current, and also feeds PV power to grid. Load power factor is 0.78 lagging and due to compensation by UPQC-DG, source power factor is found to be 0.97, which is close to unity power factor (Fig. 6.10(c) and (d)).

Load active and reactive powers in steady state are 290 W and 190 VAR respectively. In proposed method reactive power is shared as per VA ratings of converters (Table. 6.5), the reactive VARs supplied by shunt and series APFs are 125 & 52 respectively, with power angle being 16.5°. Reactive power is not fully compensated due to non-idealities and grid still supplies a very small part of reactive power. PV array power is extracted near its maximum power point and is fed through shunt APF. As shown in snapshot of control panel of PV simulator (Fig. 6.10(e)), PV array supplies 101 W, which is 98.4% of maximum power available.

6.6.2 Transient Results

Experimental validation is also carried out for transient situations of voltage sag and swell. Performance during sag is tested for a sag of 17% (due to current limitations of some equipment) and load voltage was maintained at its rated value (Fig. 6.11(a)). For voltage swell of 30% of rated voltage, load voltage was maintained within 5% of its rated value due to compensation provided by series APF (Fig. 6.11(b)). Source current remains sinusoidal and in-phase with source voltage during sag or swell.

Performance during reduction in solar irradiation (for a steep change from 100% to 20%) is shown in Fig. 6.11 (c). When PV power reduces, source current increases to keep load power constant. Shunt APF current increases to withdraw power for maintaining DC link voltage and for meeting the power losses, which were supplied by PV. Load current and grid voltage remain unaffected by change in solar PV power. Dynamic performance of UPQC-DG for voltage swell is shown in Fig. 6.11 (d). On occurrence of swell, DC voltage experiences an overshoot of 9 V (8.2%) but returns to steady state within 0.22 seconds due to PI action. Source current reduces in swell condition to keep load power constant.

During variation in solar irradiation, output power extracted from PV remains close to maximum power available at that irradiation. For solar irradiation of 500 W/m^2, PV array operating point shown in Fig. 6.12 is at 96.4% of maximum power.

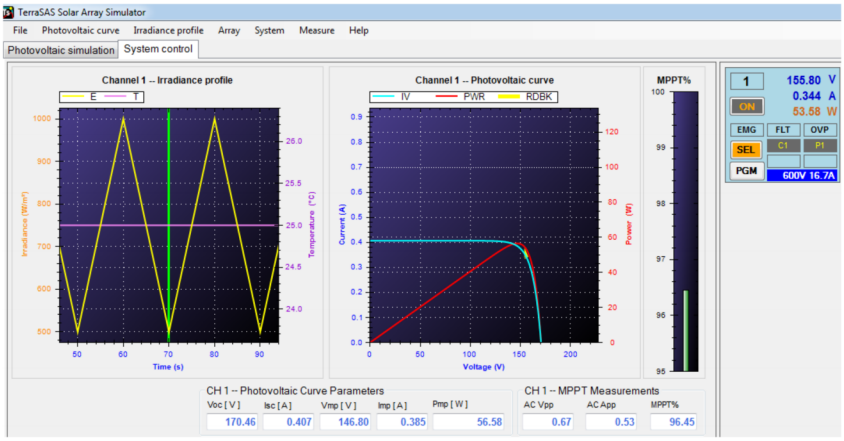

Figure 6.12: PV output power at reduced irradiation

6.7 Summary

In this chapter, VA rating of UPQC-DG has been optimized by sharing reactive power between series and shunt converters of UPQC-DG in a systematic manner. Proposed optimal UPQC-DG sizing method, which is based on improved power angle control (PAC) is found to be superior to existing PAC methods and provides 5.16% reduction in total VA rating and 7.26% reduction in total cost of UPQC-DG in comparison to the conventional method (without PAC). The cost of UPQC-DG with proposed PAC based design method is also 5.94% less than that obtained with existing PAC method. CHIL validation performed using Opal-RT, and Dspace/micro-labbox verifies that proposed power angle control, incorporating VA limiting method, makes sure that VA loadings of converters remain within designed ratings under all operating conditions of UPQC-DG, in contrast to existing PAC Method, which violates the VA ratings of converters in some of the operating conditions. Also, proposed PAC method yields better utilization of series converter of UPQC-DG in comparison to existing PAC method. Proposed control method is also validated using hardware setup of UPQC-DG for steady state as well as transient performance.

Bibliography

[1] S. Devassy and B. Singh, "Modified pq-theory-based control of solar-PV-integrated UPQC-S," *IEEE Transactions on Industry Applications*, vol. 53, no. 5, pp. 5031–5040, 2017.

[2] V. Khadkikar and A. Chandra, "UPQC- S: A novel concept of simultaneous voltage sag/swell and load reactive power compensations utilizing series inverter of UPQC," *IEEE Transactions on Power Electronics*, vol. 26, no. 9, pp. 2414–2425, 2011.

[3] A. Q. Ansari, B. Singh, and M. Hasan, "Algorithm for power angle control to improve power quality in distribution system using unified power quality conditioner," *IET Generation, Transmission & Distribution*, vol. 9, no. 12, pp. 1439–1447, 2015.

[4] A. K. Panda and N. Patnaik, "Management of reactive power sharing and power quality improvement with SRF-PAC based UPQC under unbalanced source voltage condition," *International Journal of Electrical Power & Energy Systems*, vol. 84, pp. 182–194, 2017.

[5] J. Ye, H. B. Gooi, and F. Wu, "Optimization of the size of upqc system based on data-driven control design," *IEEE Transactions on Smart Grid*, vol. 9, no. 4, pp. 2999–3008, 2018.

[6] B. B. Ambati and V. Khadkikar, "Optimal sizing of UPQC considering VA loading and maximum utilization of power-electronic converters," *IEEE Transactions on Power Delivery*, vol. 29, no. 3, pp. 1490–1498, 2014.

[7] K. Palanisamy, D. Kothari, M. K. Mishra, S. Meikandashivam, and I. J. Raglend, "Effective utilization of unified power quality conditioner for interconnecting PV modules with grid using power angle control method," *International Journal of Electrical Power & Energy Systems*, vol. 48, pp. 131–138, 2013.

[8] V. Madhaiyan and V. Subramaniam, "Extended reference signal generation scheme for integration of unified power quality conditioner in grid-connected photovoltaic system," *Electric Power Components and Systems*, vol. 43, no. 8-10, pp. 914–927, 2015.

[9] L. B. G. Campanhol, S. A. O. da Silva, A. A. de Oliveira, and V. D. Bacon, "Power flow and stability analyses of a multifunctional distributed generation system integrating a photovoltaic system with unified power quality conditioner," *IEEE Transactions on Power Electronics*, vol. 34, no. 7, pp. 6241–6256, 2018.

[10] V. Khadkikar, "Fixed and variable power angle control methods for unified power quality conditioner: operation, control and impact assessment on shunt and series inverter kVA loadings," *IET Power Electronics*, vol. 6, no. 7, pp. 1299–1307, 2013.

[11] L. B. G. Campanhol, S. A. O. da Silva, A. A. de Oliveira, and V. D. Bacon, "Single-stage three-phase grid-tied PV system with universal filtering capability applied to DG systems and AC microgrids," *IEEE Transactions on Power Electronics*, vol. 32, no. 12, pp. 9131–9142, 2017.

[12] S. Devassy and B. Singh, "Design and performance analysis of three-phase solar PV integrated UPQC," *IEEE Transactions on Industry Applications*, vol. 54, no. 1, pp. 73–81, 2018.

[13] S. J. Wright, *Primal-dual interior-point methods*. Siam, 1997, vol. 54.

[14] V. Khadkikar, P. Agarwal, A. Chandra, A. Barry, and T. Nguyen, "A simple new control technique for unified power quality conditioner (UPQC)," in *Proc. 11th IEEE International Conference on Harmonics and Quality of Power*, 2004, pp. 289–293.